Formation of pyramids and mounds in molecular beam epitaxy

Martin Siegert*
Theoretische Physik, FB 10, Universität Duisburg, 47048 Duisburg, Germany

Michael Plischke
Physics Department, Simon Fraser University, Burnaby, British Columbia, Canada V5A 1S6
(Received 22 June 1995)

One of the generic scenarios in molecular beam epitaxy is the growth of three-dimensional structures such as mounds and pyramids. These structures are a nonequilibrium effect thought to be due to a combination of the microscopic Ehrlich-Schwoebel barriers and the breaking of detailed balance by the deposition process. We propose and investigate by computer simulation a simple microscopic model that displays (i) slope selection, (ii) pyramid and moundlike structures, and (iii) coarsening. The characteristic length scale of our three-dimensional features grows as $R(t) \sim t^n$ with n between 0.17 and 0.26. We discuss these results in the light of recent experiments and continuum models of molecular beam epitaxy.

PACS number(s): 05.40.+j, 68.55.−a, 81.10.Aj, 05.70.Ln

I. INTRODUCTION

In the last few years, it has become clear that the technologically important molecular beam epitaxy (MBE) growth process can give rise to a surprising variety of different morphologies. Even in the simplest possible situation of homoepitaxial growth, one finds stable layer-by-layer growth, kinetically rough films, and, perhaps most surprisingly, unstable three-dimensional growth that can result in mounds or pyramids. This three-dimensional growth mode was first predicted by Villain [1] and later seen in computer simulations of a simple solid-on-solid (SOS) model [2]. Since then, three-dimensional growth has been observed experimentally in such diverse systems as GaAs/GaAs(001) [3,4], Cu/Cu(001) [5], Ge/Ge(001) [6], Fe/Fe(001) [7], and Fe/MgO(001) [8]. Although much experimental work remains to be done, the following features seem to be well established: (i) three-dimensional growth is a nonequilibrium effect; in the absence of deposition, the surface returns to its stable thermodynamic state which may be flat or rough [4]; (ii) during growth three-dimensional features coarsen; the characteristic lateral dimension R seems to grow with a power law $R(t) \sim t^n$ with n somewhere in the range 0.16–0.26 [5,7,8]; (iii) the slope of mounds or pyramids remains essentially constant after an initial transient [3,5,7,8]; this terminal slope is determined by material parameters and growth conditions; (iv) only certain substrate orientations support unstable growth; slightly miscut GaAs grows in the step-flow mode [9] whereas GaAs(001), under the same conditions, produces mounds [3,10]; on Cu(001) faceted pyramids with sides of orientation (115) are formed [5] but growth of Cu on Cu(115) remains stable [11].

These experimental facts can all be qualitatively explained in terms of the following theoretical considerations. Atoms diffusing on a vicinal surface experience a potential energy barrier when approaching a downward step. This barrier, commonly referred to as an Ehrlich-Schwoebel barrier [12,13] or diffusion bias [1], may be due to loss of coordination number by a diffusing atom in the vicinity of the step or to long-range strain fields. The Ehrlich-Schwoebel effect leads to preferential incorporation of diffusing atoms at upward steps or, in other words, an uphill diffusion current. It is important to recognize that this diffusion current is purely a nonequilibrium effect. In the absence of deposition, the principle of detailed balance guarantees that there cannot be a net current on a crystallographically stable facet. On the other hand, during growth, the deposition process breaks detailed balance and slope-dependent currents are generically present. One of the possible consequences of the Ehrlich-Schwoebel effect is the destabilization of a singular surface during growth: islands form and because atoms deposited on top of islands are inhibited from diffusing over the edges, islands form on top of these islands resulting in a three-dimensional structure.

From the discussion above, it is not yet clear how slope selection can occur — the scenario described potentially leads to structures that have slopes which increase indefinitely. However, there are other processes that counterbalance the Ehrlich-Schwoebel effect. For example, knockout processes described in [14,15] and exchange effects [16] both can produce diffusion currents that flow preferentially downhill. Thus it is understandable that a combination of such effects, all of which are temperature and material dependent, can lead to the selection of one or more slopes at which the net current in the *nonequi-*

*Present address: Department of Physics, Simon Fraser University, Burnaby, British Columbia, Canada V5A 1S6. Electronic address: siegert@sfu.ca

librium situation vanishes. It is, of course, also possible that a slope may be selected simply by the symmetry of the growing crystal: if the surfaces bounding the three-dimensional structure are singular surfaces then the diffusion current must be zero, and the first such surface encountered is stable.

The foregoing scenario was first proposed by Krug, Plischke, and Siegert (KPS) [17] and further developed by Siegert and Plischke [18] who, guided by the work of Johnson *et al.* [10], proposed a Langevin equation that led to the formation of pyramids with the selection of a particular slope, and coarsening of pyramids according to $R(t) \sim t^{1/4}$. Similar results have been obtained by other groups [19,7] using the same basic ideas. For completeness, we review here these continuum models. We begin with the conservation law that applies to MBE growth in the situation where there is no evaporation of particles as well as no voids or overhangs:

$$\frac{\partial h(\mathbf{r},t)}{\partial t} + \nabla \cdot \mathbf{j}(\mathbf{r},t) = F + \eta(\mathbf{r},t), \tag{1.1}$$

where $h(\mathbf{r},t)$ is the height of the surface at time t at substrate location $\mathbf{r}$, $\mathbf{j}(\mathbf{r},t)$ is the diffusion current, F is the mean deposition rate, and $\eta(\mathbf{r},t)$ is the Gaussian nonconservative noise function that describes the fluctuations in the deposition rate. To incorporate the effects of diffusion barriers and to guarantee the selection of a finite slope in the long-time limit, one uses a diffusion current which is a function of the local slope $\mathbf{m}(\mathbf{r},t) = \nabla h(\mathbf{r},t)$ and has the general form

$$\mathbf{j}(\mathbf{m}) = \mathbf{j}_b(\mathbf{m}) + D_{\rm eq}\nabla\Delta h(\mathbf{r},t)\ , \tag{1.2}$$

where the second term on the right is the leading contribution to the equilibrium current and the nonequilibrium current $\mathbf{j}_b$ has the form $j_{b,\alpha} = m_\alpha f_\alpha(\mathbf{m})$, $\alpha = 1,2$, with functions f_α that have the properties (i) $f_\alpha(\mathbf{0}) > 0$ in order to destabilize a singular surface and (ii) $f_\alpha(\mathbf{m}_0) = 0$ for some finite $\mathbf{m}_0$, and, in the case of cubic symmetry, $f_\alpha(-\mathbf{m}) = f_\alpha(\mathbf{m})$, $f_1(m_1,m_2) = f_2(m_2,m_1)$ [20]. Similar conditions apply in the case of other lattice symmetries. Taking the gradient of both sides of Eq. (1.1) then produces a Langevin equation for the two-component order parameter $\mathbf{m}$ which resembles that used to describe domain growth in a magnet with a conserved order parameter below its critical point [15]:

$$\frac{\partial \mathbf{m}(\mathbf{r},t)}{\partial t} = -D_{\rm eq}\Delta\Delta\mathbf{m} + \nabla[\nabla\cdot\mathbf{j}_b] + \nabla\eta(\mathbf{r},t). \tag{1.3}$$

In the one-dimensional case, where the order parameter is a scalar, this analogy is exact since the right-hand side may be written as the functional derivative of a "free energy" with respect to m plus conservative noise. For nonzero noise, it is known [21] that this equation produces domain growth with a characteristic time dependence $R(t) \sim t^{1/3}$. In two dimensions, three features spoil the analogy: (i) it is no longer possible, in general, to derive the diffusion current from a free energy function, (ii) even if such a free energy exists, the order parameter $\mathbf{m} = \nabla h$ and therefore $\nabla \times \mathbf{m} = \mathbf{0}$, a condition not normally applicable to the order parameter of a magnet and, (iii) the interchange of divergence and gradient in the second term on the right produces an extra coupling between the two components of the order parameter. In this list, conditions (ii) and (iii) are important and conspire to produce a slower growth of domains than in the magnetic case: instead of the well-known Lifshitz-Slyozov-Wagner law $R(t) \sim t^{1/3}$ for a magnetic system with a finite number of equivalent ground states, one finds $R(t) \sim t^n$ where $n \leq 0.25$ [18,19,7].

Several authors have studied three-dimensional growth using versions of this continuum formalism. Johnson *et al.* [10] used a spherically symmetric function $f_{1,2} = f(m^2)$ that does not have a nontrivial zero and, therefore, no slope selection. Hunt *et al.* [19] used the one-dimensional version of the same current and found coarsening with $n \approx 0.22$. Stroscio *et al.* [7] modified the *equilibrium current* by discarding the leading contribution $D_{\rm eq}\nabla\Delta h(\mathbf{r},t)$ and retaining the next available linear term, containing five derivatives of $h(\mathbf{r},t)$, in an attempt to reduce the value of n. The integration of their Langevin equation produced $n \approx 0.18$. At this stage, it is fair to say that no fundamental understanding of the quantitative difference between domain growth in magnets and MBE exists. We also note that a very similar Langevin equation describes the spinodal decomposition of an unstable crystal facet [22,23] and growth exponents in the same range have been found in this context [23].

In this article, we discuss a complementary approach to the study of unstable three-dimensional growth, namely, the investigation of microscopic models that contain both the destabilizing Ehrlich-Schwoebel effect and a counterbalancing downhill current that results in slope selection. An atomistic model with Ehrlich-Schwoebel barriers has been previously used to study the early stages of three-dimensional growth by Šmilauer *et al.* [24] but this model may not display slope selection.

The remainder of this article is organized as follows. In Sec. II we describe our model for three-dimensional growth. Results for both "pyramids" and "mounds" are discussed in Sec. III. We then discuss (Sec. IV) the nontrivial issue of how one can distinguish experimentally the situation of extreme kinetic roughening as described, e.g., by the Mullins-Herring equation, from the case of unstable three-dimensional growth. We also discuss various crossover phenomena that can complicate a comparison of theory and experiment. We conclude, in Sec. V, with a brief summary and an outlook for future theoretical and experimental work.

II. THE MODEL

We consider a simple solid-on-solid model in which particles are deposited at a rate $f = \tau_{\rm dep}^{-1}$ on an initially flat substrate in the form of a square lattice of adsorption sites. Deposition is random and particles attach only to the tops of existing columns, thus ensuring that there are no voids or overhangs. Between deposition events, par-

ticles that are not completely buried attempt to hop to the top of a randomly selected nearest-neighbor column. This diffusion process is controlled by a local energy function and the hopping probabilities obey detailed balance. The energy of a particle at the top of the column at location $\mathbf{r}$ is taken to be

$$E(\mathbf{r}) = -E_1 n_1(\mathbf{r}) - E_b n_2(\mathbf{r}), \tag{2.1}$$

where $n_1(\mathbf{r})$ is the number of lateral nearest neighbors of the particle at $\mathbf{r}$ and $n_2(\mathbf{r})$ is the number of particles in the neighboring columns that are either one step above or below $h(\mathbf{r})$. In order to implement diffusion bias, together with the activated hopping that is commonly used to model surface diffusion, we choose our hopping rates in the following way:

$$W\left[h(\mathbf{r}) \to h(\mathbf{r}) - 1, h(\mathbf{r}') \to h(\mathbf{r}') + 1\right] = \frac{1}{\tau_{\mathrm{dif}}} \exp\left[-\frac{E_1}{k_B T} n_1(\mathbf{r})\right] W_b\left[n_2(\mathbf{r}') - n_2(\mathbf{r})\right], \tag{2.2}$$

where

$$W_b\left[n_2(\mathbf{r}') - n_2(\mathbf{r})\right] = \begin{cases} \exp\left(-\frac{E_b}{k_B T}\left[n_2(\mathbf{r}) - n_2(\mathbf{r}')\right]\right), & n_2(\mathbf{r}) > n_2(\mathbf{r}') \\ 1, & n_2(\mathbf{r}) \le n_2(\mathbf{r}'). \end{cases} \tag{2.3}$$

The second part, W_b, of the hopping rates incorporates the effects of the step-edge barriers into the diffusion process: If an adatom approaches the step edge from above, the number of next-nearest-neighbor bonds is reduced and the move is suppressed by a factor $\sim \exp[-E_b/(k_B T)]$. The expression for W_b is the standard Metropolis transition probability and reflects the fact that the hopping rate from site $\mathbf{r}$ to $\mathbf{r}'$ depends on the energy barrier between the two states. This, in turn, is given by the maximum of the potential energy of the intermediate states. Thus the hopping rates must depend on the *direction* of the move — something that is missing in the simple form of the Arrhenius-type hopping rate that forms the first part of Eq. (2.2) which depends only on the bond configuration of the *initial* site. Physically the form chosen for W_b means that an adatom that diffuses over the step-edge barrier from above passes through an intermediate state directly at the top of the step edge. The corresponding energy barrier to reach that state is E_b. The adatom hops away from that state with probability one. We note that a very similar diffusion algorithm has already been used in Ref. [24].

In a Monte Carlo simulation the attempt frequencies τ_{dif} and τ_{dep} are not independent parameters: the ratio $\tau_{\mathrm{dep}}/\tau_{\mathrm{dif}} = (1-f)/f$ corresponds to the ratio D/F of the diffusion constant of adatoms to the deposition flux in an experiment. Only this ratio enters into the Monte Carlo simulation; the common prefactor of the attempt frequency only sets the time scale. This prefactor is furthermore modified by a factor $\exp[-E_0/(k_B T)]$: The barrier E_0 for the diffusion of an adatom on a flat terrace again influences only the time scale and therefore has been omitted in the argument of the exponential in (2.2). In the remainder of this article we will use the number of deposited monolayers as a natural unit of time.

In some of our simulations, we have also introduced anisotropy into the diffusion process. Such anisotropy is known to be important on a number of semiconductor surfaces and is presumably responsible for the elongated moundlike structures seen in GaAs [9,25]. In our model, we have simply made the second-neighbor interaction strongly anisotropic: we have only added the contribution proportional to E_b for neighboring columns in the $\pm x$ directions. The diffusion process then still obeys detailed balance but now provides some smoothening in the y direction while inhibiting the approach to a downward step from the x direction.

In order to stabilize the three-dimensional structures at some finite slope we also introduce a slope-dependent downhill current to counteract the effects of the diffusion bias. While we could easily incorporate knockout processes or exchange effects into the model, we have chosen to simply generate downhill currents in the deposition step. We allow a fraction p of the deposited particles to immediately hop to a nearest-neighbor column of lower height, if one exists. Without diffusion, this deposition process is the two-dimensional version of a model first investigated by Family [26], that is well known to be in the universality class of the Edwards-Wilkinson (EW) equation [27]:

$$\frac{\partial h(\mathbf{r},t)}{\partial t} = \nu(p)\Delta h(\mathbf{r},t) + \eta(\mathbf{r},t), \tag{2.4}$$

where the coefficient ν obviously increases as a function of p. Comparing with Eq. (1.1) we see that this process contributes a downhill current $\mathbf{j} = -\nu(p)\mathbf{m}$ to the diffusion current.

The model, as described above, contains a number of parameters. We have adjusted these so as to obtain (i) unstable growth for reasonably small substrate sizes L and (ii) to obtain steady-state profiles that have slopes small enough to be consistent with the SOS approximation. Point (i) refers to the fact that the Mullins-Herring term $\Delta\Delta\mathbf{m}$ suppresses the instability for small enough system sizes. In the linear approximation, Eqs. (1.1), (1.2) take the form

$$\frac{\partial h(\mathbf{r},t)}{\partial t} = -\nu_2 \Delta h(\mathbf{r},t) - D_{\mathrm{eq}} \Delta\Delta h(\mathbf{r},t) + \eta(\mathbf{r},t)$$

and it is clear that this equation has a band of unstable modes for wave vectors $k < \sqrt{\nu_2/D_{\mathrm{eq}}}$. Thus in a discrete system of dimension L, there will be unstable growth only if $L > 2\pi\sqrt{D_{\mathrm{eq}}/\nu_2}$. Since the dynamic exponent $z \approx 4$ in these models, it is only possible to simulate rather small systems for the times required to reach the steady state. For these reasons, we have chosen, if not noted otherwise, $f = 0.01$, $p = 0.1$ or 0.25, $E_1/(k_B T) = 1$, and $E_b/(k_B T) = 5$. These parameters are far from being realistic for real materials but do allow us to exhibit the effects of interest for substrate sizes as small as $L = 64$.

These are the basic ingredients of the model. The cal-

culations of surface currents to be described at the beginning of the next section have been performed on substrates of size 64×64 with helical boundary conditions to impose an overall tilt. All other simulations were performed with periodic boundary conditions for $L \times L$ substrates with $L \leq 128$. As we show in the next section, this basic model leads to the formation of pyramids with "facets" in the $\langle 11n \rangle$ directions where n is determined by the competition between the stabilizing and destabilizing currents or, in the case of anisotropic diffusion, to mounds with ridges aligned in the y direction. These structures are, of course, not smooth as there is still the ordinary kinetic roughening superimposed on the three-dimensional steady-state shape.

III. RESULTS

We first discuss the case of pyramid formation. To make the connection with the continuum theory [18,15] we first use the method introduced by KPS [17] to measure the surface diffusion currents. Since the facets of the evolving pyramids grown on a flat substrate turn out to be oriented in $\langle 11n \rangle$ directions (see below) we measure the surface current on substrates tilted in these directions. The results for several values of the knockout probability p and the deposition rate f are shown in Fig. 1. For $f = 0.01$ and $p = 0$ [Fig. 1(a)] the surface current has a zero at the rather large slope $m_0 \simeq 1.6$ [$\mathbf{m}_0 \simeq (1.1, 1.1)$]. As expected, a nonzero knockout probability pushes the zero to smaller values of m [see Fig. 1(b) for $p = 0.25$]. A reduction of the deposition rate f leads to a larger diffusion length $l_d \sim [(1-f)/f]^{\chi}$; the exponent χ depends on the actual mechanism of island formation in the submonolayer regime and lies between 1/6 and 1/2 [28]. According to Ref. [18] a larger value of l_d manifests itself in a shift of the maximum of the $j(m)$ curve to smaller values of m that is clearly seen in Fig. 1(c). Interestingly the position of the zero in $j(m)$ is basically independent of the flux f. This agrees with the idea [18] that the selected slope is determined by material properties of the growing film.

The appearance of a zero in $\mathbf{j}(\mathbf{m})$ at a nonzero slope for $p = 0$ is at first glance surprising since there is no explicit mechanism for a downhill component of the diffusion current. To see that special large-slope configurations can contribute to a negative current, we consider the following surface profile in one dimension: $h(0) = h(1) = 0$, $h(2) = 2$, $h(3) = 3$, $h(4) = 4$. The particle at the double step at $x = 2$ has $n_2(2) = 2$, the same second-neighbor coordination number that it will have if it hops to $x = 1$. On the other hand, if it hops to $x = 3$ it will have $n_2(3) = 1$. Therefore for this configuration $W[h(2) \to 1, h(1) \to 1] = \exp\{E_b/(k_BT)\} W[h(2) \to 1, h(3) \to 4]$ and we have an example of a preferential downhill hopping rate. Diffusion dynamics on slopes $\mathbf{m} = (m_1, m_2)$ with $m_i > 1$ are not described realistically in a SOS model as overhangs would naturally occur. However, the occurrence of slopes $m = |\mathbf{m}| > \sqrt{2}$ with $j(m) > 0$ in the model with $p = 0$ is not only a failure of the SOS condition, but, more seriously, also a failure of modeling surface dynamics on a simple cubic lattice. If the diffusion dynamics were modeled on more realistic lattice geometries the much richer set of high symmetry orientations would introduce additional zeros of the surface diffusion current and therefore would effectively suppress the occurrence of overhangs. Keeping this in mind the micro-

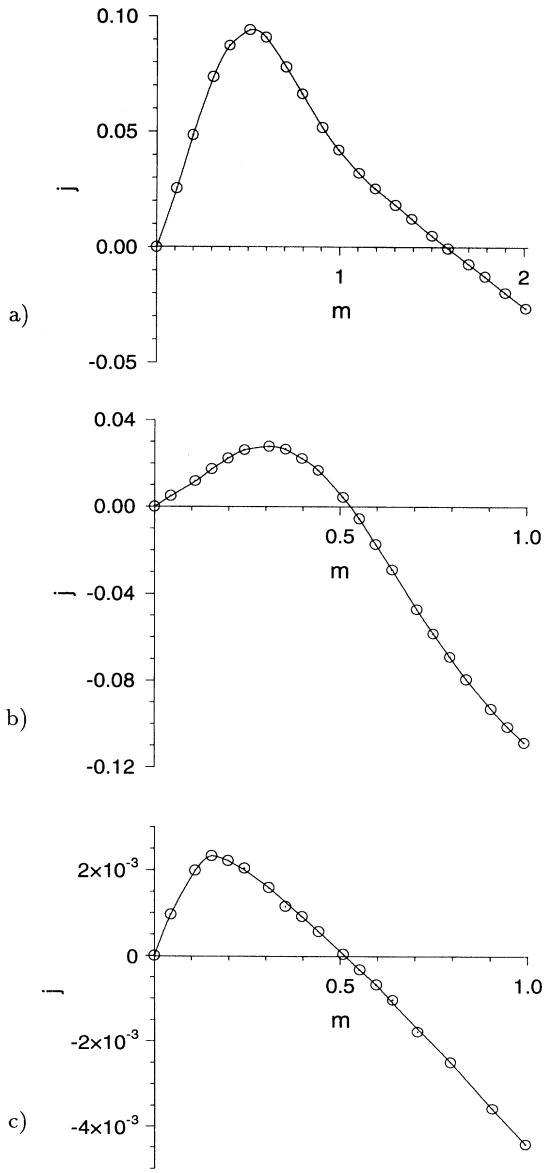

FIG. 1. Surface diffusion currents on substrates tilted in the $(11n)$ direction: (a) $p = 0$, $f = 0.01$, (b) $p = 0.25$, $f = 0.01$, and (c) $p = 0.25$ and $f = 10^{-4}$. The other parameters are $E_1/(k_BT) = 1$ and $E_B/(k_BT) = 5$. In (a) and (b) the currents have been averaged over the first 20 deposited monolayers and 1000 independent runs, whereas in (c) the average has been performed only over the first 20 monolayers and 100 independent runs. The solid lines are drawn as a guide to the eye (arbitrary dimensionless units).

scopic dynamics of this model for large slopes should not be regarded as a true description of the dynamics for a real material, but as an effective model for additional high symmetry surfaces that cannot be described correctly on a simple cubic lattice that is used for reasons of computational efficiency only.

The foregoing argument shows that for the particular implementation that we have chosen for the Ehrlich-Schwoebel barriers there are configurations that contribute a downhill component to the diffusion current if the slope becomes large enough, i.e., if there are at least some steps of height 2. We are, of course, unable to calculate the current $\mathbf{j}(\mathbf{m})$ from the microscopic dynamics — there is no general method that reliably produces the correct continuum version of a microscopic model [20,29]. However, the above example at least makes it plausible that for large slopes $\mathbf{j}(\mathbf{m})$ may have a zero even for $p = 0$.

The theory of Siegert and Plischke [18] predicts that film growth on singular surfaces under conditions typical for MBE leads to the formation of pyramidlike structures. The slopes of the sides of the pyramid are determined by the zeros of the surface current. In principle we could choose any of the parameter sets used in Fig. 1. However, from a simulational point of view a large value of m_0 has several disadvantages: First, since m_0 determines the selected tilt of the sides of the pyramids, a value of $m_0 > 1$ is not consistent with the solid-on-solid condition of our model because overhangs are expected to become important at these angles. Second, it takes a fairly long time until that selected slope is built up. This leads to an extensive crossover regime until the asymptotic regime is reached, where the slopes are basically constant and the surface evolution proceeds through a coarsening process. Similarly, small values of the flux f require an enormous amount of computer time so that it is hard to reach the asymptotic regime as well. For these reasons most of our simulations of pyramid formation have been done with the parameter set used in Fig. 1(b). We emphasize that this choice is dictated by the need of computational efficiency, not by physical reasons. For example, a flux $f = 0.01$ is unrealistically large and consequently the surface morphology obtained in these simulations cannot be compared with morphologies seen in real experiments. A much better agreement is obtained for a flux $f = 10^{-4}$. In Fig. 2 we show typical surface morphologies for film thicknesses of 140 and 2000 deposited monolayers that are quite similar to the morphologies seen in experiments [7,8]. As already mentioned above, the sides of the pyramids are oriented in the $\langle 11n \rangle$ directions. The simplest form of a diffusion current (1.2) that would generate such morphologies uses functions $f_1(\mathbf{m}) = f(m_1)$ and $f_2(\mathbf{m}) = f(m_2)$ with $f(m_0) = 0$. In this case the selected slopes are simply $(\pm m_0, \pm m_0)$. In Fig. 2(c) we also show a cut through the film that illustrates the slope selection during the growth process. If the average slope $|\mathbf{m}|$ is estimated from the straight parts in Fig. 2(c) one obtains a value in the range of 0.55–0.66 that agrees well with the zero of the surface current in Fig. 1(c) [30].

We use the local slope $\mathbf{m}$ of the surface as an order-parameter to characterize to the surface morphology. To be specific we use the first zero $R_1(t)$ of the order param-

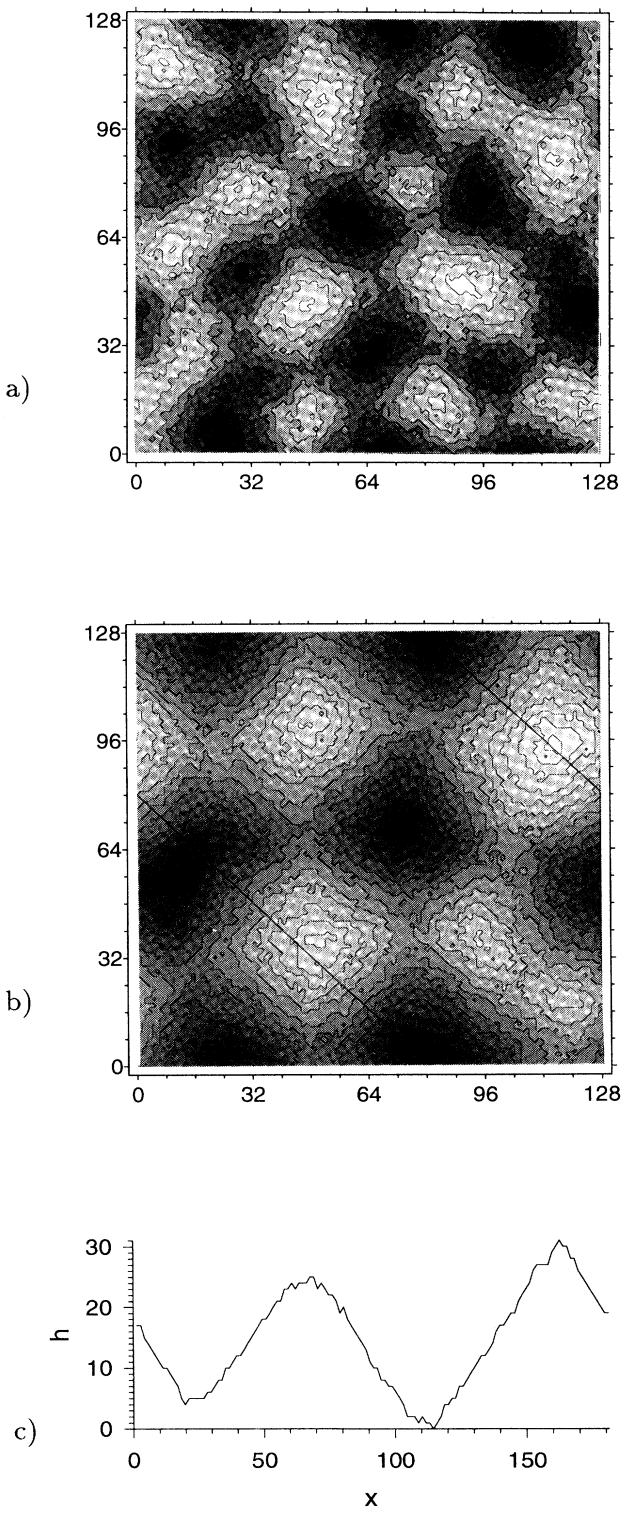

FIG. 2. Contour plots of surface morphologies for (a) 140 and (b) 2000 deposited monolayers; $f = 10^{-4}$, $p = 0.25$, $E_1/(k_BT) = 1$, $E_b/(k_BT) = 5$. In (c) a cut through the film along the line indicated in (b) is shown that emphasizes the slope selection in the profile. The selected slope corresponds to the zero in Fig. 1(c).

eter correlation function

$$C(\mathbf{r},t) = \langle \mathbf{m}(\mathbf{r},t)\mathbf{m}(\mathbf{0},t)\rangle \tag{3.1}$$

to describe the coarsening process of the pyramid formation quantitatively. The angular brackets in (3.1) indicate averaging over choice of origin as well as over different Monte Carlo runs. In Fig. 3 we show our results for two different deposition rates, $f = 0.01$ and $f = 10^{-4}$. Time is measured in numbers of deposited monolayers. For $f = 0.01$ we obtain an almost perfect power law, $R_1(t) \sim t^{0.26}$ over almost five decades in very good agreement with the continuum theory [18]. For $f = 10^{-4}$ the behavior is more complex. The diffusion length l_d determines the average distance between nucleation sites in the submonolayer growth regime. Since this is the same as the average island size before the coalescence of islands sets in, l_d also sets the initial size, respectively, base, of the pyramids. In other words, at least initially the size of the pyramids is proportional to l_d and therefore decreases with f. This is clearly seen in Fig. 3. It follows that initially the tilt of the pyramids for small f is much smaller than the selected slope m_0 that corresponds to the zeros of the surface current $\mathbf{j}$. Thus there will be a crossover regime where the slope of the pyramids increases until it reaches its asymptotic value m_0. These crossover effects will be discussed further in Sec. IV. However, this simple argument already shows that the value of $n = 0.26$ obtained for $f = 0.01$ is much closer to the asymptotic value than the effective exponents that can be extracted from Fig. 3 for $f = 10^{-4}$.

Also included in Fig. 3 are results for the square of the local slope $\langle \mathbf{m}^2(t)\rangle \equiv C(\mathbf{0},t)$. Since the slope behaves like an order parameter in a magnetic system with conserved dynamics [18,15] this quantity should converge to a constant. This is the basic mechanism for the slope selection. For $f = 0.01$ $\langle \mathbf{m}^2(t)\rangle$ becomes basically constant within the first few monolayers, whereas for $f = 10^{-4}$ the convergence is obtained only after the deposition of more than 200 monolayers. Unfortunately, $\langle \mathbf{m}^2(t)\rangle$ is *not* a measure for the selected slope: The selected slope m_0 is obtained in the limit $\lim_{\mathbf{r}\to 0} C(\mathbf{r},t) = \langle \mathbf{m}(t)\rangle^2$ that is always smaller than $C(\mathbf{0},t)$ because of fluctuations. This explains the discrepancy between the asymptotic value obtained for $\langle \mathbf{m}^2(t)\rangle$ from Fig. 3 and the slopes seen in Fig. 2(c), respectively, the value m_0 measured in Fig. 1. This is also apparent from the fact that the asymptotic value of $\langle \mathbf{m}^2(t)\rangle$ for $f = 10^{-4}$ is smaller than the value obtained for $f = 10^{-2}$. Clearly, the fluctuations have to be smaller for smaller deposition rates, whereas, as mentioned above, the location of the zero in the surface current is basically independent of f.

We now turn to the case of anisotropic diffusion where the second-neighbor interaction acts only in the x direction. In Fig. 4 we show a single configuration grown for 0.1×2^{16} monolayers on a 64×64 substrate for $p = 0.1$. This picture clearly shows a three-dimensional structure predominantly characterized by the wave vector $\mathbf{k} = \frac{2\pi}{L}(1,0)$ and an average slope $\bar{\mathbf{m}} \approx (2/3, 0)$. In Fig. 5 we show the steady-state structure factor $S(\mathbf{k}) = \langle h(\mathbf{k})h(-\mathbf{k})\rangle$, where $h(\mathbf{k})$ is the Fourier transform of the height function $h(x,y)$, averaged over ten samples and plotted for $\mathbf{k} = (k_x, 0)$ and $(0, k_y)$. The structure factor $S(0,k_y)$ seems to display conventional kinetic roughening in this stable direction. For small k_y a reasonable fit to a power law is obtained, $S(0,k_y) \sim k_y^{-\gamma_y}$ with $\gamma_y \approx 2.5$. At this point we have no theory that predicts this exponent. In the unstable x direction, the structure factor is best described as a smooth function of k_x for large k_x on which is superimposed the power spectrum of the selected shape. This shows up primarily in the smallest three values of k_x. In this range of k_x, the structure factor $S(k_x,0)$ increases by more than three orders of

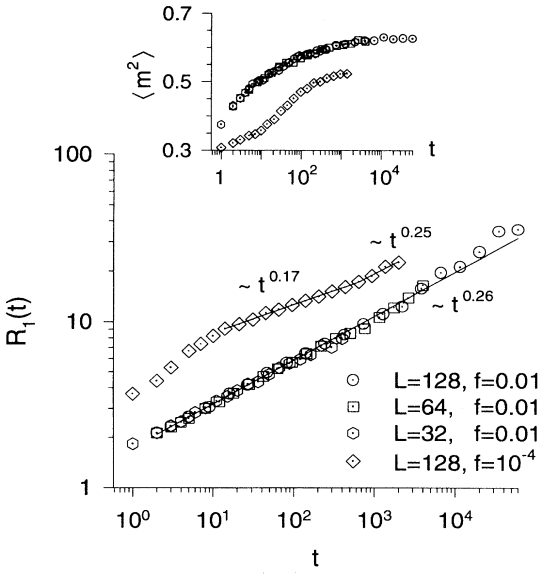

FIG. 3. First zero $R_1(t)$ of the slope-slope correlation function $C(\mathbf{r},t)$ (3.1) for two different deposition rates. The straight lines correspond to power-law fits with the indicated exponents. The inset shows the square of the order parameter $\langle \mathbf{m}^2(t)\rangle \equiv C(\mathbf{0},t)$ for the same parameter sets.

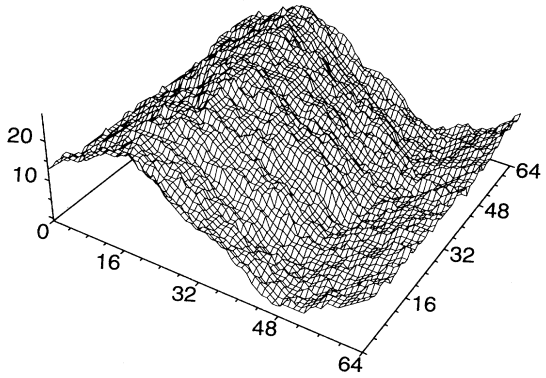

FIG. 4. Snapshot of the surface $h(x,y,t)$ as a function of substrate position (x,y) of a film grown on a 64×64 substrate for a time $t = 0.1 \times 2^{16}$ deposited monolayers with anisotropic Schwoebel barriers.

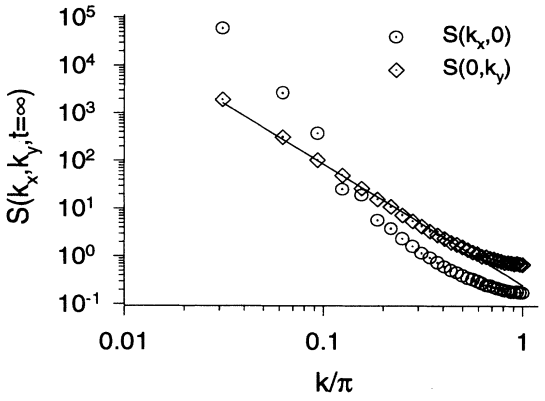

FIG. 5. Steady-state structure factor for $L = 64$ for the case of anisotropic diffusion. The straight line is a fit to the functional form $S(0, k_y) = Ak_y^{-\gamma_y}$ and yields $\gamma_y \approx 2.5$. The function $S(k_x, 0)$ does not show power-law behavior: to see this one would have to subtract the steady-state profile from the height $h(x, y, t)$ [2].

magnitude.

We next discuss the behavior of the order parameter and the coarsening of the mounds. We characterize the unstable growth process using the equal-time correlation functions

$$C_{\alpha\alpha}(x, y) = \langle m_\alpha(x, y, t) m_\alpha(0, 0, t) \rangle , \qquad (3.2)$$

with $\alpha = x, y$. In Fig. 6 we show the correlation functions $C_{xx}(x, 0)$ and $C_{xx}(0, y)$ for $L = 128$ and $t = 0.1 \times 2^{17}$ monolayers averaged over 15 samples. At this time, the size of the mounds in the transverse y direction has reached the size of the system as indicated by the fact that $C_{xx}(0, y)$ does not cross zero. The fact that this function reaches a finite asymptotic value at $y = L/2$ also shows that the mounds are well oriented along the y direction. The function $C_{xx}(x, 0)$, on the other hand, has well-defined oscillations and the locations of the zeros $R_j(t)$ of this function provide convenient measures of the width of the mounds. From the graph we see that even at the late time used, there are still at least two mounds present — for a single mound, as shown in Fig. 4 for $L = 64$, the first zero R_1 of $C_{xx}(x, 0)$ appears at $R_1 = L/4$.

One can use any of the zeros of $C_{xx}(x, t)$ to study the growth of the mounds as a function of time. It turns out that the second zero $R_2(t)$ provides the most stable estimate. The reason is that there is a large discontinuity in $C_{xx}(x, t)$ between $x = 0$ and $x = 1$ — the square of the nearest-neighbor step height $C_{xx}(0, t)$ is considerably larger than the extrapolated value $\lim_{x\to 0} C_{xx}(x, t)$. Moreover, at intermediate times, when the mounds are already well established, the short-range correlation function can be negative for $x \leq 3$ even though there is a finite average slope. These effects tend to make the determination of $R_1(t)$ less reliable than that of $R_2(t)$. In Fig. 7 we show the time dependence of $R_2(t)$ for $L = 64$ and $L = 128$. The data are reasonably well fitted with a power law $R_2(t) \sim t^n$ with $n \approx 0.18$ over three decades in time for $L = 128$ and over a shorter interval for $L = 64$. The behavior of the other characteristic lengths $R_1(t)$ and $R_3(t)$ is entirely consistent with this result. We have also examined the growth of the mounds in the y direction. This overlaps the coarsening process: The characteristic length of the mounds becomes significant long before they begin to coarsen and becomes equal to the substrate size for $L = 128$ at $t < 10^5$.

Although the fit of $R_2(t)$ to a power law, as shown in Fig. 7, is quite good, there are indications that the actual functional form may be more complicated. This is illustrated in Fig. 8 where we plot the square of the width as a function of time for $L = 64$ and $L = 128$. Although the form $W^2(t) = 0.22t^{0.52}$ provides a reasonable fit to the data over the same time interval in which coarsening occurs, one can see significant deviations from a pure power law. Moreover, one might also expect that $W^2 \sim t^{2\beta} \sim R_1^2 C_{xx}(0, t)$. If one fits $C_{xx}(0, t)$ (also shown in Fig. 7) to a power law one obtains a very

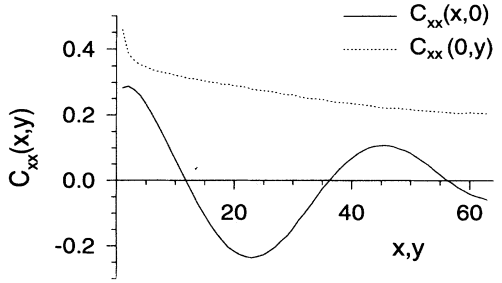

FIG. 6. Correlation functions $C_{xx}(x, 0, t)$ and $C_{xx}(0, y, t)$ for $L = 128$ and $t = 0.1 \times 2^{17}$ monolayers.

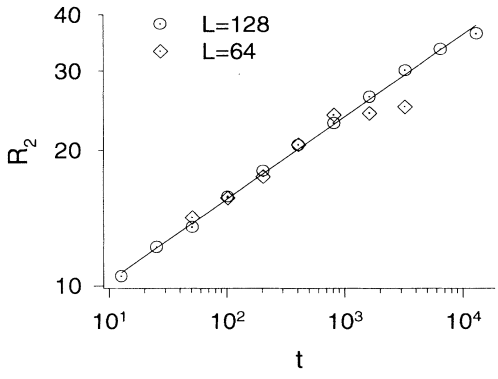

FIG. 7. Evolution of the characteristic size of the mounds in the case of anisotropic Schwoebel barriers for $L = 64$ and $L = 128$. The straight line is a fit to the form $R_2(t) = At^n$ and yields $n \approx 0.18$.

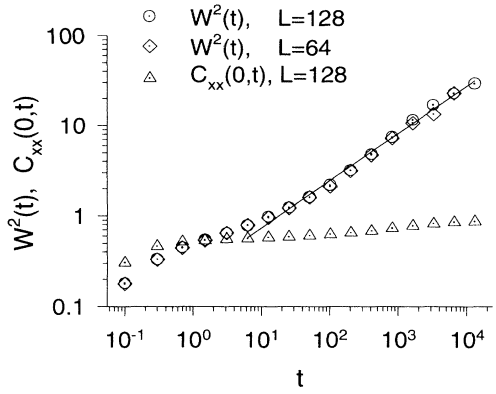

FIG. 8. Plot of the square of the width of the interface as a function of time for anisotropic diffusion and $L = 64$ and $L = 128$. The straight line is a fit to the form $W^2(t) = Bt^{2\beta}$ and yields $\beta \approx 0.26$ over the same time interval in which the mounds coarsen. Also shown is the mean square nearest-neighbor step height in the x direction $C_{xx}(0,0,t)$.

small exponent $C_{xx}(0,t) \sim t^{0.06}$ and therefore an estimate $2\beta \approx 0.42$ which is well outside the uncertainty in the direct estimate of the exponent β. Similar deviations from pure power-law behavior are also seen in integrations of Langevin equations of the type (1.3) [15] and this remains to be understood.

IV. CROSSOVER BEHAVIOR AND COMPARISON WITH EXPERIMENT

The result that the pyramid size grows $\sim t^{1/4}$ may, depending on parameters such as temperature, flux, etc., be seen only after the deposition of many monolayers. The growth behavior for earlier times can be influenced by crossover effects that make the comparison of theory with experiment more complicated. Quite generally, we observe that crossover effects always lead to effective growth exponents $n < 1/4$. This is the case for numerical solutions of Langevin equations of type (1.3) as well as for the Monte Carlo simulations. The only exceptions from this rule appear during the deposition of the first few monolayers as seen in Fig. 3 for $f = 10^{-4}$.

First, we discuss crossover effects in the context of the Langevin equation (1.1) with a surface current

$$j_{b,\alpha} = D_b m_\alpha (1 - u m_\alpha^2) \ , \quad \alpha = 1,2 \ . \tag{4.1}$$

Since all constants $D_{\rm eq}$, D_b, u can be scaled out of the problem [31,15] the extent of the crossover regime of the equation of motion [32]

$$\frac{\partial h}{\partial t} = -\Delta\Delta h - \nabla \cdot \mathbf{j}_b + \sqrt{\epsilon}\,\eta \tag{4.2}$$

depends only on the single remaining parameter, the noise strength $\epsilon \sim Fu/D_{\rm eq}$. In Fig. 1 we saw that small deposition rates, i.e., small noise strength in the framework of Langevin equations, have a second effect: they lead to a shift of the maximum of the $\mathbf{j}(\mathbf{m})$ curve to smaller tilts. This cannot be modeled with the current (4.1). Instead one can use the current

$$j_{b,\alpha} = \frac{m_\alpha (1 - m_\alpha^2)}{(1 - m_\alpha^2)^2 + (l_d m_\alpha)^2} \ , \quad \alpha = 1,2 \tag{4.3}$$

that was proposed in Ref. [18]. The additional parameter, the diffusion length l_d, fixes the position of the maximum at $\simeq 1/l_d$. In Fig. 9 results for the first zero $R_1(t)$ of the height-height correlation function from a numerical integration [33] of Eq. (4.2) are shown for the current (4.1) with $\epsilon = 0$ and $\epsilon = 1$, and for the current (4.3) with $\epsilon = 0$ and $l_d = 10$. For noise strength $\epsilon = 1$ we obtain a power-law increase $\sim t^n$ with $n \simeq 0.23$ that is within the error bars of $n = 1/4$. For the same form (4.1) of the current, but $\epsilon = 0$, the exponent $n \simeq 0.21$ is only slightly smaller. The largest deviation $n \simeq 0.20$ from $n = 1/4$ is obtained for the current (4.3) with $l_d = 10$. The importance of larger values of the diffusion length l_d is also seen in the behavior of the order parameter $\langle \mathbf{m}^2 \rangle$ shown in the inset of Fig. 9: Whereas for the current (4.1) $\langle \mathbf{m}^2 \rangle$ does not change very much after a short initial period, there is a substantial variation in the average slope over four decades in time for $l_d = 10$. We believe that effective values $n < 1/4$ are in most cases related to situations where the average slope has not yet saturated.

In the framework of Monte Carlo simulations the crossover behavior can be characterized quite similarly. As already mentioned in Sec. III, almost no crossover is seen for high deposition rates corresponding to large noise strengths ϵ (see Fig. 3, $f = 0.01$). For $f = 10^{-4}$

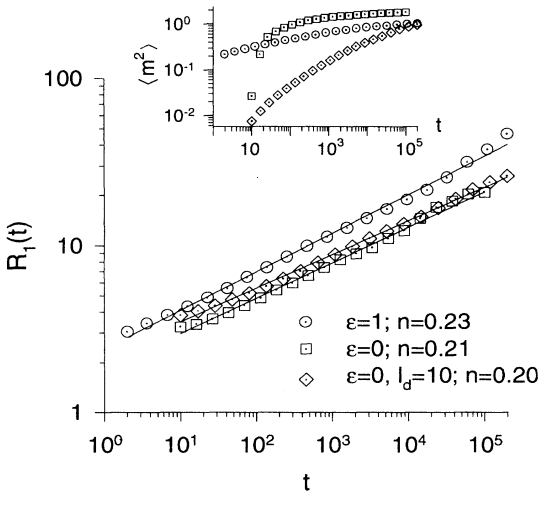

FIG. 9. First zero $R_1(t)$ of the slope-slope correlation function $C(\mathbf{r},t)$ obtained from a numerical integration of Eq. (4.2); the squares (circles) correspond to the current (4.1) for noise strengths $\epsilon = 0$ ($\epsilon = 1$), the diamonds correspond to the current (4.3) with $\epsilon = 0$ and $l_d = 10$. The straight lines are power-law fits $R_1(t) \sim t^n$. The exponent n is listed in the legend. The inset shows the behavior of the averaged square of the slope $\langle \mathbf{m}^2(t) \rangle$ for the same parameters.

there is a large regime, $t \simeq 10 - 600$ monolayers, that is characterized by a much slower growth, $\beta_{\rm eff} \simeq 0.17$. In the same regime the average slope still increases as seen from the behavior of $\langle \mathbf{m}^2(t) \rangle$. Only after the deposition of more than 600 monolayers does the growth seem to cross over to the asymptotic regime with $R_1(t) \sim t^{1/4}$. Effective exponents around 0.17 have also been observed in the growth of Fe on Fe(001) [7]. In that case the slower growth has been attributed to the absence of thermal excitations and consequently to the absence of the Mullins term $D_{\rm eq}\Delta\Delta h$ in the corresponding equation of motion. In our Monte Carlo simulations with $E_1/(k_B T) = 1$ such thermal excitations are certainly present and therefore the slower growth must have a different origin. In the discussion of the Langevin equation (4.2) we also saw that smaller growth exponents can be obtained even if the Mullins term is present.

We have seen that unstable growth leading to pyramid formation can be most easily characterized by means of surface currents that generically have the form shown in Fig. 1. Since surface currents as a function of the tilt can hardly be measured in an experiment, other quantities must be studied to classify the growth behavior. Whereas kinetic roughening is characterized by *two* exponents, the roughness exponent ζ and the dynamical exponent z, the growth exponent $\beta = 1/z$ is the only exponent present in the case of pyramid formation ($\zeta = 1$). Thus for $\zeta < 1$ a measurement of the roughness exponent may be sufficient to distinguish between the two scenarios. If $\zeta = 1$, the comparison is more complicated as the scaling form of, e.g., the height-height correlation function

$$G(\mathbf{r}, t) = \langle [h(\mathbf{r}, t) - h(\mathbf{0}, t)]^2 \rangle \sim r^2 f(r/R(t)) \qquad (4.4)$$

is identical in the two cases. In the case of kinetic roughening this behavior follows from the standard scaling assumption [34] and the characteristic length $R(t) \sim t^{1/z}$ is the correlation length $\xi(t)$, whereas in the case of pyramid formation the scaling form (4.4) is obtained from the scaling behavior of the slope-slope correlation function

$$C(\mathbf{r}, t) = c(r/R(t)) \qquad (4.5)$$

that behaves like the order-parameter correlation function in systems that phase order as in spinodal decomposition or Ostwald ripening. In this case the typical length scale corresponds to the pyramid size. Surfaces that can be described within the theory of kinetic roughening are scale invariant on scales smaller than the correlation length, whereas this is not necessarily true in the case of pyramid formation. However, this difference is difficult to quantify, in particular, as even in the deterministic process of pyramid formation, kinetic roughness is superimposed on the growing structures. We will show that the two different scenarios can be most easily distinguished by looking at the *form* of the correlation functions. To be specific we compared our results for pyramidal growth obtained from Langevin equations (1.1) and Monte Carlo simulations with the results for kinetic roughening following from the linear equation

$$\frac{\partial h}{\partial t} = -\Lambda\Delta\Delta h + \eta \; . \qquad (4.6)$$

Note, however, that there is no theoretical justification, nor do we intend to imply that Eq. (4.6) describes kinetic roughening in materials correctly. To describe a realistic situation, several nonlinear terms have to be added to the right-hand side of Eq. (4.6) that would change the growth exponents [29]. In particular, there is no reasonable theory of kinetic roughening that predicts a roughness exponent $\zeta = 1$ for two-dimensional surfaces as Eq. (4.6) does. In fact, we believe that all experiments in which roughness exponents in the range $\zeta \simeq 0.7 - 1.0$ have been measured can be explained in terms of pyramid formation. This is elucidated in Fig. 10, where the height-height correlation function obtained from Eq. (4.2) with $\mathbf{j}_b$ from (4.1) and $\epsilon = 1$ is plotted. If these results were interpreted within the theory of kinetic roughening, one would extract an effective roughness exponent $\zeta \simeq 0.8$ from the small distance behavior. The results for larger film thicknesses also show that this effective value for ζ slowly increases. Clearly, the asymptotic result must be $\zeta = 1$ for the equations describing pyramid formation. Therefore measurements for the growth of Ag on Ag(111) [35], in which exponents $\zeta = 0.8$ and $\beta = 0.25$ have been obtained, are in almost perfect agreement with the theory of pyramid formation although the results were originally interpreted within the framework of kinetic roughening. These deviations from the r^2 behavior for small r are quite generic and can be traced back to the nonzero noise strength; similar deviations are also found in the results of our Monte Carlo simulations. In our numerical integrations of the Langevin equation (4.2) for $\epsilon = 0$ we find basically no deviations from the r^2 behavior for either current (4.1) or (4.3). As an aside, we mention that the exponent $\beta = \zeta/z$ should not be used to describe pyramidal growth although one may argue that effectively we have $\zeta = 1$ for pyramid formation and therefore the exponent β is formally identical with $n \equiv 1/z$. However, the underlying physical mechanism is totally different, and,

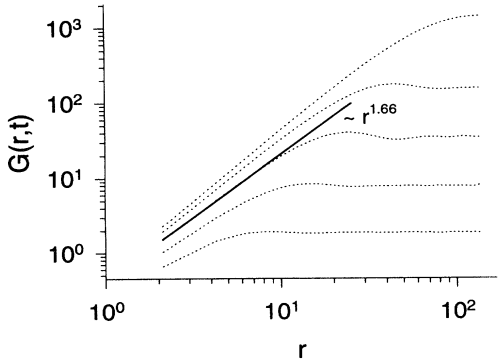

FIG. 10. Height-height correlation function $G(\mathbf{r}, t)$ obtained from a numerical integration of Eq. (4.2) with $\mathbf{j}_b$ from Eq. (4.1) and $\epsilon = 1$ (dotted lines). The straight line corresponds to a power-law fit $G \sim r^{2\zeta}$ with $\zeta = 0.83$. For later times (upper curves) this effective value of ζ increases.

as already mentioned, kinetic roughness is usually superimposed on the pyramids. If the exponent β is defined to characterize the increase of the surface width and the exponent n to describe the growth of the pyramid size that corresponds to the wavelength of the oscillations of the height-height or slope-slope correlation functions then, as explained at the end of the preceding section, the exponent β must be always larger than n.

As explained in the preceding paragraph, we use the linear equation (4.6) only to clarify the differences between kinetic roughening and pyramid formation. For this purpose Eq. (4.6) is particularly simple as all correlation functions can be calculated analytically. Usually the height-height correlation function is evaluated by fitting a power law to the data for distances smaller than the correlation length ξ as has been done in Fig. 10. On the other hand, the differences between pyramid formation and kinetic roughening become most apparent on length scales *larger* than the correlation length: In the case of pyramid formation the height-height correlation function has an oscillatory behavior and the wavelength of the oscillations is determined by the pyramid size. As well, the correlation functions become anisotropic: If the correlation function is measured in the $\langle 110 \rangle$ directions we expect for quadratic pyramids a wavelength that is larger by a factor of $\sqrt{2}$ in comparison with the wavelength measured in the $\langle 100 \rangle$ directions. In the case of kinetic roughening the correlation functions are roughly constant on scales larger than ξ. The oscillatory behavior becomes more apparent when the height-height correlation function is plotted on a *linear scale, not, as it is usually done, on a log-log scale that suppresses the oscillations.* These differences can be seen even more clearly by studying the slope-slope correlation functions. In Fig. 11 we compare the results for Eq. (4.6) with the Monte Carlo results described in this article. Whereas for early times it is hard to notice a difference between the two cases, the oscillatory behavior of the slope-slope correlation function in the case of pyramid formation [Fig. 11(b)] becomes apparent for larger film thicknesses.

In Fig. 11(b) we also indicate the limiting behavior of the correlation function for $r \to 0$: For $r > \sqrt{2}a$, a being the lattice constant, the plotted lines coincide with the actual values of the measured correlation function. For $r \leq \sqrt{2}a$ the values of the correlation functions are indicated by symbols, whereas the lines are extrapolated to zero by fitting the correlation function to a cosine times an exponential function [36]. The extrapolated values $\lim_{\mathbf{r}\to 0} C(\mathbf{r},t) = \langle \mathbf{m}(t) \rangle^2$ are roughly a factor of 2–4 smaller than the measured value of $C(\mathbf{0},t) = \langle \mathbf{m}^2(t) \rangle$. For 1370 deposited monolayers (ML) the average slope is almost saturated, and we obtain from the extrapolated values an estimate $\langle \mathbf{m}(t) \rangle \simeq 0.53$ that is in excellent agreement with the zero of the surface current [see Fig. 1(c)]. Since the form of the correlation function is expected to be universal, an estimate of the average slope $\langle \mathbf{m}(t) \rangle$ can in principle also be obtained from the first minimum of the correlation function that is quite easy to measure. For our Monte Carlo simulations with $f = 10^{-4}$ we find for late times a ratio $\langle \mathbf{m}(t) \rangle^2 / [-C_{\min}(t)] \simeq 2.1$.

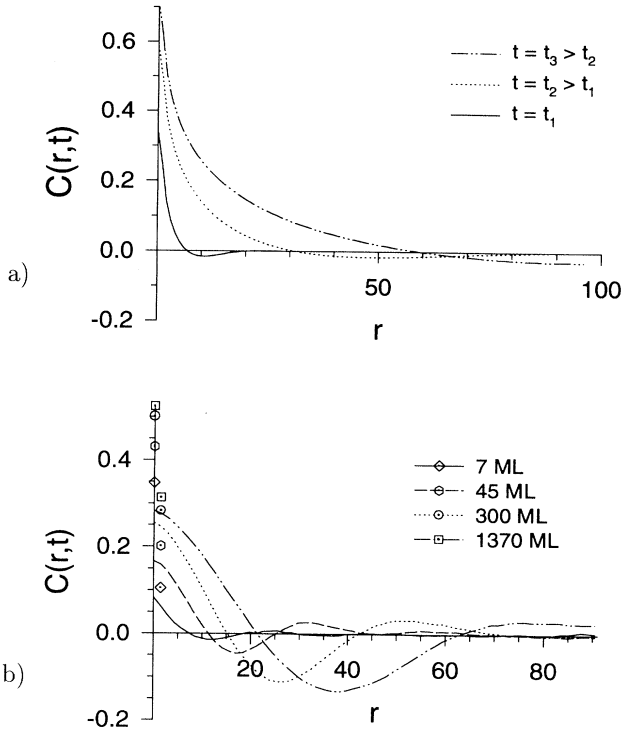

FIG. 11. Comparison of the slope-slope correlation functions for (a) kinetic roughening with $\zeta = 1$ and (b) pyramid formation, $f = 10^{-4}$. For small times (solid lines) the differences in the form of the correlation function are small, whereas for larger film thicknesses (dotted and dashed-dotted lines) the oscillatory behavior in the case of pyramid growth becomes apparent. In (b) the difference between $C(\mathbf{0},t)$ (symbols) and $\lim_{\mathbf{r}\to 0} C(\mathbf{r},t)$ (lines) is also indicated (see text).

For the numerical integrations of the Langevin equation (4.2) with $\epsilon = 0$ we find a ratio of roughly 1.6. However, we also find that ratio increases with the noise strength so that this way of estimating the average slope seems to be less practical.

Theory predicts that the selected slopes of the evolving pyramids are given by the zeros of the surface current. These surface orientations correspond to the stable solutions of the equation of motion (1.1). This means that if Eq. (1.1) is linearized around these zeros the Edwards-Wilkinson equation is obtained. This point has been verified by Ernst and co-workers. In their first experiment Cu was deposited on Cu(001) [5] and for $T = 220$ K pyramids with side planes corresponding to $\{115\}$ orientations were observed. In a later experiment [11] Cu was deposited on Cu(115) at the same temperature and no instability was observed in agreement with the theoretical ideas.

V. CONCLUSIONS

In this article we have shown that the Ehrlich-Schwoebel effect combined with nonconservative noise generi-

cally leads to the formation of three-dimensional structures that progressively coarsen as a function of time and saturate at a stable, substrate-size-independent form. Previous simulations of a related model [24] have shown the destabilizing of a singular surface but our models are the first [37] to display the slope selection predicted on the basis of general arguments [17,18]. For the case of isotropic diffusion and symmetric Ehrlich-Schwoebel barriers, the steady-state morphologies are pyramids as are found experimentally in the case of homoepitaxy on Cu(001). We have also shown that for substrates which give rise to anisotropic diffusion, the steady-state shapes are elongated "mounds," reminiscent of those seen in experiments on GaAs [9,4], rather than the symmetric pyramids mentioned above.

We have also studied the coarsening of the mounds and pyramids and found that the characteristic length scale grows as a function of deposition time according to $R(t) \sim t^n$ with $n \approx 0.25$ in the case of pyramids and $n \approx 0.18$ for mounds. In the case of mounds, the crossover effects are considerably larger than in the case of pyramids and it is by no means clear that the difference between the two exponents will survive when larger systems are studied.

We have also discussed in some detail the interpretation of experimental data. Because the exponent ζ, which characterizes the growth of the height-height correlation function at short distances, is equal to one in the case of pyramid growth and is also equal to one in the linear Mullins-Herring equation, which is often taken to be a starting point for theories of MBE, some care must be taken in the analysis of data for very rough interfaces ($\zeta \approx 1$). We have shown that one way to distinguish unambiguously between kinetically very rough interfaces and unstable three-dimensional growth is to examine the *shape* of the height-height or slope-slope correlation function. For the case of kinetic roughening, these functions saturate as a function of separation whereas they oscillate in the case of pyramid formation. We note that these correlation functions should be accessible through scanning tunneling microscopy.

Finally, we mention that a major unresolved question remains, namely, the relation of unstable growth as described here to the coarsening found in phase ordering. The characteristic exponent $n \leq 0.25$ is significantly smaller than the $n = 1/3$ of the Lifshitz-Slyozov-Wagner coarsening although the Langevin equations describing these two processes are quite similar, although not identical. The elucidation of this difference as well as the development of models that incorporate proper parameters for specific materials should form a fruitful area of research for some time to come.

ACKNOWLEDGMENTS

We thank Joachim Krug, Pavel Šmilauer, Dietrich Wolf, and Andy Zangwill for helpful discussions and/or correspondence. This research was supported by the Deutsche Forschungsgemeinschaft under Grant No. SFB 166 and by the NSERC of Canada.

[1] J. Villain, J. Phys. (France) I **1**, 19 (1991).

[2] M. Siegert and M. Plischke, Phys. Rev. Lett. **68**, 2035 (1992). We note that the microscopic model used in this reference is not very realistic in describing the evolution of large slopes. However, the potential energy affecting an adatom on a vicinal surface in this model is very similar to that that is usually used to model diffusion on a vicinal surface with Ehrlich-Schwoebel barriers. Thus the onset of the instability is described correctly. In fact, the measured surface diffusion current [17] has the same form that was later proposed in Ref. [10].

[3] G. W. Smith, A. J. Pidduck, C. R. Whitehouse, J. L. Glasper, and J. Spoward, J. Cryst. Growth **127**, 966 (1993).

[4] C. Orme, M. D. Johnson, K. T. Leung, and B. G. Orr, in *Compound Semiconductor Epitaxy*, edited by C. W. Tu, L. A. Kolodziejski, and V. R. McCrary, MRS Symposia Proceedings No. 340 (Materals Research Society, Pittsburgh, 1994), p. 233.

[5] H.-J. Ernst, F. Fabre, R. Folkerts, and J. Lapujoulade, Phys. Rev. Lett. **72**, 112 (1994).

[6] J. E. Van Nostrand, S. J. Chey, M.-A. Hasan, D. G. Cahill, and J. E. Greene, Phys. Rev. Lett. **74**, 1127 (1995).

[7] J. A. Stroscio, D. T. Pierce, M. Stiles, A. Zangwill, and L. M. Sander (unpublished).

[8] K. Thürmer, R. Koch, M. Weber, and K. H. Rieder, Phys. Rev. Lett. **75**, 1767 (1995).

[9] C. Orme, M. D. Johnson, J. L. Sudijono, K. T. Leung, and B. G. Orr, Appl. Phys. Lett. **64**, 860 (1994).

[10] M. D. Johnson, C. Orme, A. W. Hunt, D. Graff, J. Sudijono, L. M. Sander, and B. G. Orr, Phys. Rev. Lett. **72**, 116 (1994).

[11] H.-J. Ernst (private communication).

[12] G. Ehrlich and F. G. Hudda, J. Chem. Phys. **44**, 1039 (1966); S. C. Wang and G. Ehrlich, Phys. Rev. Lett. **70**, 41 (1993).

[13] R. L. Schwoebel and E. J. Shipsey, J. Appl. Phys. **37**, 3682 (1966); R.L. Schwoebel, J. Appl. Phys. **40**, 614 (1969).

[14] D. D. Vvedensky, A. Zangwill, C. N. Luse, and M. R. Wilby, Phys. Rev. E **48**, 852 (1993).

[15] M. Siegert, in *Scale Invariance, Interfaces, and Non-Equilibrium Dynamics*, Vol. 344 of *NATO Advanced Study Institite, Series B: Physics*, edited by A. J. McKane, M. Droz, J. Vannimenus, and D. Wolf (Plenum, New York, 1995), pp. 165–202.

[16] G. L. Kellogg and P. J. Feibelman, Phys. Rev. Lett. **64**, 3143 (1990); G. L. Kellogg, *ibid.* **70**, 1631 (1993).

[17] J. Krug, M. Plischke, and M. Siegert, Phys. Rev. Lett. **70**, 3271 (1993).

[18] M. Siegert and M. Plischke, Phys. Rev. Lett. **73**, 1517

(1994).
[19] A. W. Hunt, C. Orme, D. R. M. Williams, B. G. Orr, and L. M. Sander, in *Scale Invariance, Interfaces, and Non-Equilibrium Dynamics*, Vol. 344 of *NATO Advanced Study Institite, Series B: Physics* [15], pp. 249-259.
[20] M. Siegert, Habilitationsschrift, Gerhard-Mercator-Universität Duisburg, 1995.
[21] T. Kawakatsu and T. Munakata, Prog. Theor. Phys. **74**, 11 (1985).
[22] J. Stewart and N. Goldenfeld, Phys. Rev. A **46**, 6505 (1992).
[23] F. Liu and H. Metiu, Phys. Rev. B **48**, 5808 (1993).
[24] P. Šmilauer, M. R. Wilby, and D. D. Vvedensky, Phys. Rev. B **47**, 4119 (1993).
[25] C. Orme, M. D. Johnson, K.-T. Leung, B. G. Orr, P. Šmilauer, and D. Vvedensky, J. Cryst. Growth **150**, 128 (1995).
[26] F. Family, J. Phys. A **19**, L441 (1986).
[27] S. F. Edwards and D. R. Wilkinson, Proc. R. Soc. London, Ser. A **381**, 17 (1982).
[28] S. Stoyanov and D. Kashiev, in *Current Topics in Materials Science*, edited by E. Kaldis (North-Holland, Amsterdam, 1981), Vol. 7, pp. 69–141; J. A. Venables, G. D. Spiller, and M. Hanbücken, Rep. Prog. Phys. **47**, 399 (1984); J. A. Blackman and A. Wilding, Europhys. Lett. **16**, 115 (1991); J. Villain, A. Pimpinelli, L.-H. Tang, and D. E. Wolf, J. Phys. (France) I **2**, 2107 (1992); M. Bartelt and J. W. Evans, Phys. Rev. B **46**, 12 675 (1992); Surf. Sci. **298**, 421 (1993); J. A. Stroscio and D. T. Pierce, Phys. Rev. B **49**, 8522 (1994); C. Ratsch, A. Zangwill, P. Šmilauer, and D. D. Vvedensky, Phys. Rev. Lett. **72**, 3194 (1994); C. Ratsch, P. Šmilauer, A. Zangwill, and D. D. Vvedensky, Surf. Sci. Lett. **329**, L599 (1995); M. Schroeder and D. E. Wolf, Phys. Rev. Lett. **74**, 2062 (1995).
[29] M. Siegert and M. Plischke, Phys. Rev. E **50**, 917 (1994).
[30] It is not completely clear that the value of m_0 measured in Fig. 1(c) has to coincide with the selected slope in Fig. 2(c): The currents plotted in Fig. 1(c) were obtained from early-time measurements (20 deposited monolayers). For a direct comparison with Fig. 2(c) it would be necessary to calculate the steady-state currents. However, this is not feasible for several reasons: In the unstable regime, $0 < m < 1/l_d$, steady-state currents can only be measured on very small substrates because otherwise a state with a constant slope in that range is unstable. For larger slopes such a measurement is possible in principle [17], but requires an enormous amount of computer time. For these reasons the agreement of the results obtained from Fig. 1(c) and Fig. 2(c) is indeed satisfactory.
[31] M. Grant, M. San Miguel, J. Viñals, and J. D. Gunton, Phys. Rev. B **31**, 3027 (1985).
[32] The height h in Eq. (4.2) is measured in a comoving frame of reference so that the flux does not appear explicitly.
[33] For a description of the numerical method see Ref. [15].
[34] F. Family and T. Vicsek, J. Phys. A **18**, L75 (1985).
[35] G. Palazantzas and J. Krim, Phys. Rev. Lett. **73**, 3564 (1994).
[36] In the case of a magnetic system with conserved order parameter the limiting behavior of the order-parameter correlation function, $C(x) \simeq 1 - [\frac{2}{\pi(d-1)}]^{1/2} x + \cdots$, is known as Porod's law [G. Porod, Kolloid Z. **124**, 83 (1951); **125**, 51 (1952)]. In the case of pyramid formation it is not known whether Porod's law holds. In particular, it is unknown whether $C(r)$ depends linearly or quadratically on r for small r. In fact, our results obtained from the integration of the Langevin equation (4.2) indicate that Porod's law does not hold, i.e., $C(r,t)$ seems to be a quadratic function of r for small r. In order to extract the limit $\lim_{r\to 0} C(r) = \langle m \rangle^2$ we have allowed for linear terms in the correlation function, however, the result does not seem to depend very much on this detail.
[37] P. Šmilauer and D. D. Vvedensky [HLRZ Jülich report, 1995 (unpublished)] investigate a similar model with emphasis on the early-time regime.

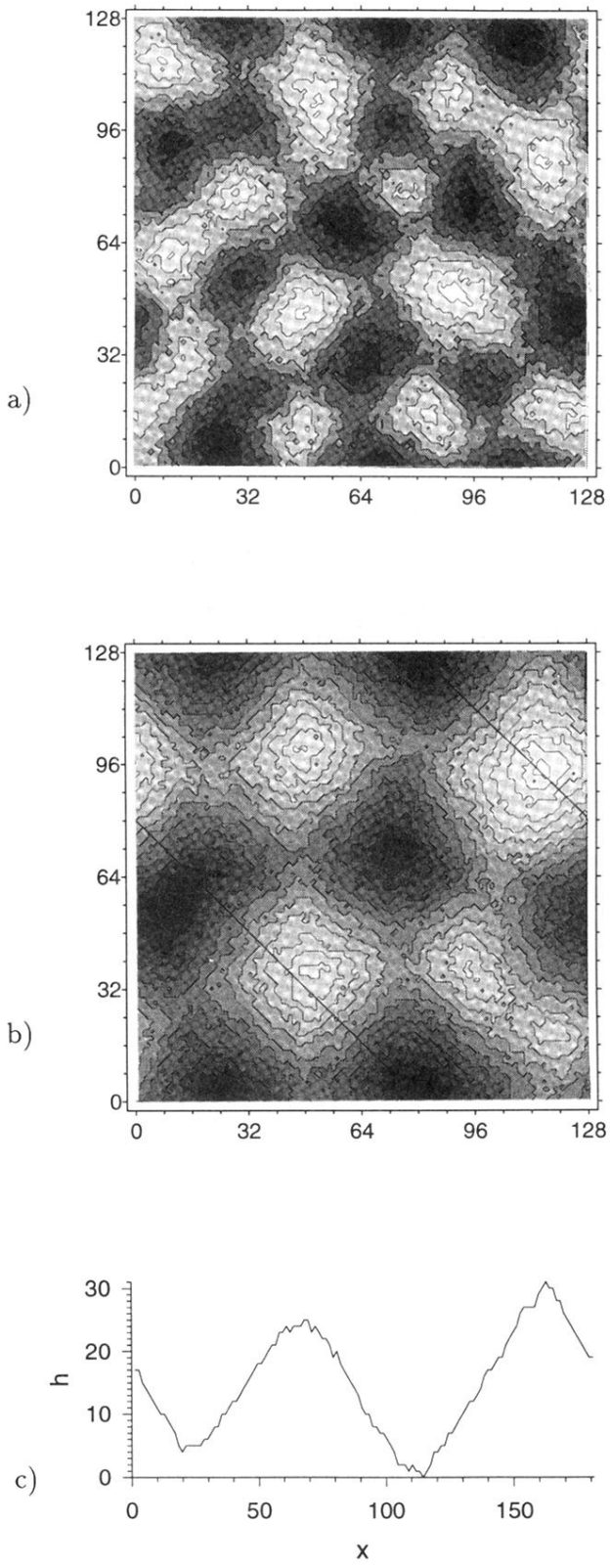

FIG. 2. Contour plots of surface morphologies for (a) 140 and (b) 2000 deposited monolayers; $f = 10^{-4}$, $p = 0.25$, $E_1/(k_BT) = 1$, $E_b/(k_BT) = 5$. In (c) a cut through the film along the line indicated in (b) is shown that emphasizes the slope selection in the profile. The selected slope corresponds to the zero in Fig. 1(c).